GEOPHYSICAL RESEARCH LETTERS, VOL. 36, L19605, doi:10.1029/2009GL040008, 2009

Zonal surface wind jets across the Red Sea due to mountain gap forcing along both sides of the Red Sea

Houshuo Jiang,[1] J. Thomas Farrar,[2] Robert C. Beardsley,[2] Ru Chen,[2,3] and Changsheng Chen[4]

Received 9 July 2009; revised 17 August 2009; accepted 31 August 2009; published 10 October 2009.

[1] Mesoscale atmospheric modeling over the Red Sea, validated by in-situ meteorological buoy data, identifies two types of coastal mountain gap wind jets that frequently blow across the longitudinal axis of the Red Sea: (1) an eastward-blowing summer daily wind jet originating from the Tokar Gap on the Sudanese Red Sea coast, and (2) wintertime westward-blowing wind-jet bands along the northwestern Saudi Arabian coast, which occur every 10–20 days and can last for several days when occurring. Both wind jets can attain wind speeds over 15 m s^{-1} and contribute significantly to monthly mean surface wind stress, especially in the cross-axis components, which could be of importance to ocean eddy formation in the Red Sea. The wintertime wind jets can cause significant evaporation and ocean heat loss along the northeastern Red Sea coast and may potentially drive deep convection in that region. An initial characterization of these wind jets is presented. **Citation:** Jiang, H., J. T. Farrar, R. C. Beardsley, R. Chen, and C. Chen (2009), Zonal surface wind jets across the Red Sea due to mountain gap forcing along both sides of the Red Sea, *Geophys. Res. Lett.*, *36*, L19605, doi:10.1029/2009GL040008.

1. Introduction

[2] The Red Sea is a meridionally-elongated oceanic basin between the African and Asian continents. It has a length of roughly 2250 km and a maximum width of 355 km. The Red Sea is surrounded by arid land, desert and semi-desert [*Naval Oceanography Command Detachment*, 1993]. Mountain chains of various altitudes rise just a short distance inland along almost the entire length of the sea. The complex orography includes a series of mountain gaps along both sides of the Red Sea (Figure 1). For example, a major gap (~110 km wide), called the Tokar Gap, is located in the Red Sea Hills, ~50 km inland from the Tokar delta on the Red Sea coast of Sudan (Figure 1a).

[3] The above-mentioned geographical features of the region are known to greatly influence surface winds over the Red Sea. In general, the high mountains on both sides of the basin orographically constrain the monthly mean surface winds to blow approximately parallel to the longitudinal axis of the Red Sea [*Patzert*, 1974]. North of 19°–20°N, the winds blow toward the southeast throughout the year, despite that the weather pattern shifts seasonally from intense thermal heat lows in summer to mid-latitude features in winter [*Naval Oceanography Command Detachment*, 1993]. South of 19°–20°N, the surface winds are controlled by the two distinct seasons of the Arabian Monsoon [*Pedgley*, 1974; *Patzert*, 1974; *Clifford et al.*, 1997; *Sofianos and Johns*, 2003]. The surface winds alternate seasonally between northwestward blowing during the Northeast Monsoon (December to March) and southeastward blowing during the Southwest Monsoon (June to September).

[4] In summer, the Tokar Gap frequently channels strong winds onto the sea surface, at times causing dust storms spreading over the southern Red Sea [*Hickey and Goudie*, 2007]. In winter, the Tokar Gap funnels winds out of the Red Sea surface [*Pedgley*, 1974, Figure 1]. It is thus evident that the surface winds can be altered by the gap to travel along curved trajectories other than simply down the main axis [*Clifford et al.*, 1997]. A series of mountain gaps also exists along the eastern side of the Red Sea (Figure 1c), and their effects on the Red Sea surface winds remain largely unknown, or at least, undocumented.

[5] Along the Red Sea coasts, there are usually strong desert-land/sea-surface temperature contrasts and large cross-shore diurnal temperature gradients. As a result, ageostrophic nighttime land breezes and daytime sea breezes occur almost daily and in all months [*Pedgley*, 1974]. Depending on locality and season, intensities of the (seaward) land breezes may be reinforced through interaction with mountain gaps and with synoptic and large-scale atmospheric circulations, leading to strong cross-axis surface winds.

[6] Within the basin the Red Sea hosts an active, complex and three-dimensional water circulation pattern [*Sofianos and Johns*, 2007]. A quasi-permanent cyclonic gyre is present in the northernmost Red Sea [*Clifford et al.*, 1997; *Sofianos and Johns*, 2007], whereas a series of strong anticyclones has been observed in summer in the central part of the Red Sea with maximum currents on the order of 1 m s^{-1} [*Sofianos and Johns*, 2007]. Other along-axis hydrographic surveys, mostly conducted in winter months, also revealed that the Red Sea is rich in eddy activity with anticyclonic dominance [*Quadfasel and Baudner*, 1993]. These eddies or sub-gyres are not permanent but tend to reemerge at preferential latitude bands [*Clifford et al.*, 1997], suggesting that their formation and evolution may be a response to strong and variable wind stress curl [*Quadfasel and Baudner*, 1993; *Sofianos and Johns*, 2007].

[7] Aside from a few robust and qualitative features (i.e., the along-axis tendency, the Tokar Gap winds, and strong

[1]Department of Applied Ocean Physics and Engineering, Woods Hole Oceanographic Institution, Woods Hole, Massachusetts, USA.
[2]Department of Physical Oceanography, Woods Hole Oceanographic Institution, Woods Hole, Massachusetts, USA.
[3]MIT-WHOI Joint Program in Oceanography, Woods Hole Oceanographic Institution, Woods Hole, Massachusetts, USA.
[4]School for Marine Science and Technology, University of Massachusetts-Dartmouth, New Bedford, Massachusetts, USA.

0094-8276/09/2009GL040008$05.00

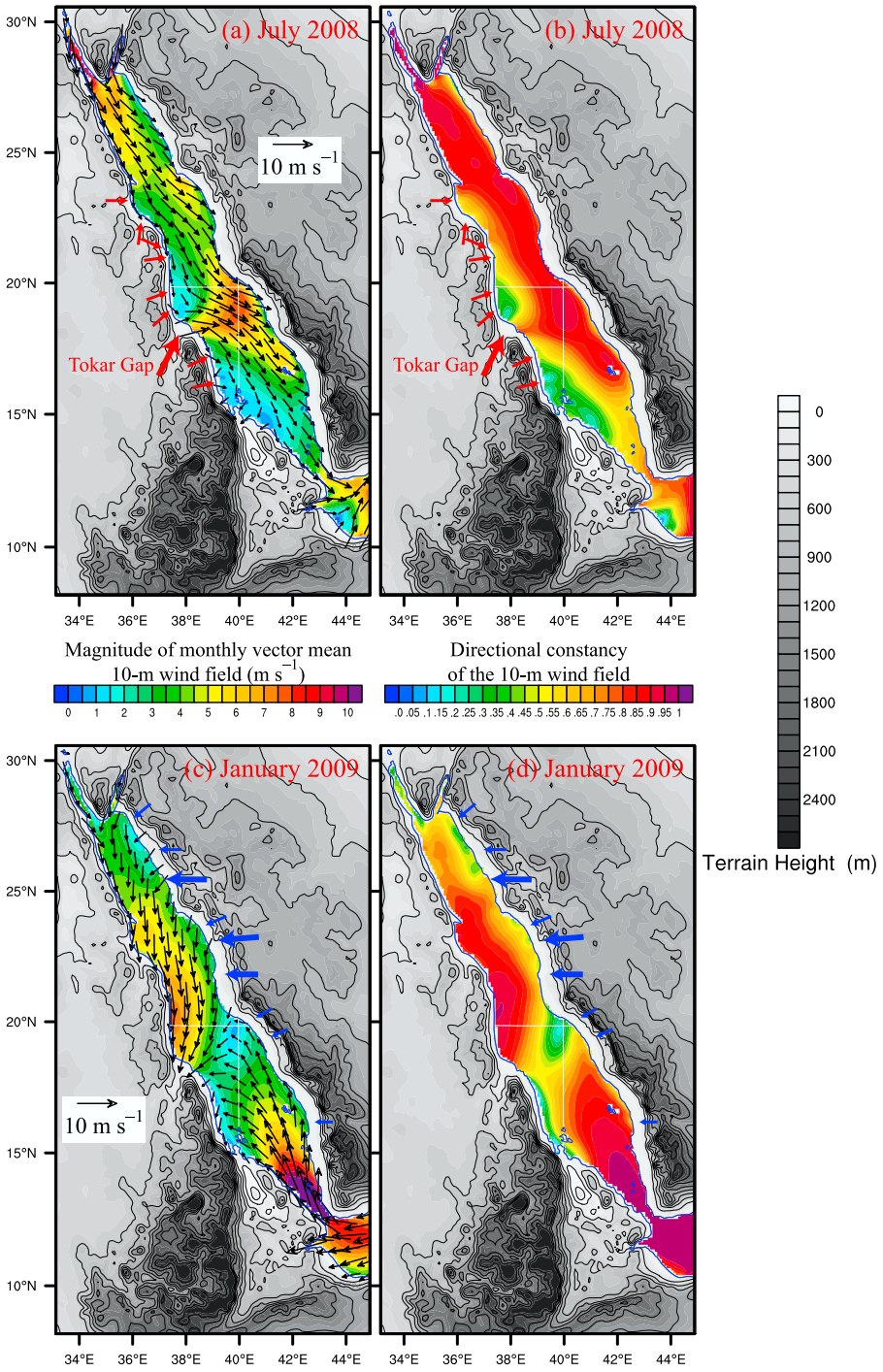

Figure 1. Monthly means of 10-m surface winds over the Red Sea from hourly WRF model output. (a) July 2008 monthly vector mean 10-m surface wind vector field overlapped with its magnitude (color contours). (b) July 2008 monthly mean 10-m wind directional constancy (color contours), defined as the ratio of the magnitude of the monthly mean 10-m wind vector to the monthly mean 10-m wind speed. (c)–(d) Same as Figures 1a–1b but for January 2009. The red (blue) arrows in Figures 1a–1b (Figures 1c–1d) indicate the locations of mountain gaps along the western (eastern) coast of the Red Sea. The wind vectors are shown for ~30 % of the grid points.

land/sea breezes), there is little quantitative knowledge of the wind field over the Red Sea, both in terms of its climatology and its spatiotemporal variability. Recent ocean model studies of the Red Sea circulation [*Sofianos and Johns*, 2002, 2003] and studies seeking to estimate the evaporation rate [*Tragou et al.*, 1999] have used climatological monthly-mean winds derived from COADS [*da Silva et al.*, 1994], which exhibit almost no cross-axis component or cross-axis variation [e.g., *Sofianos and Johns*, 2003, Figure 2]. Another general circulation model study of the Red Sea water circulation [*Clifford et al.*, 1997] used wind analysis fields from the Navy Operational Regional

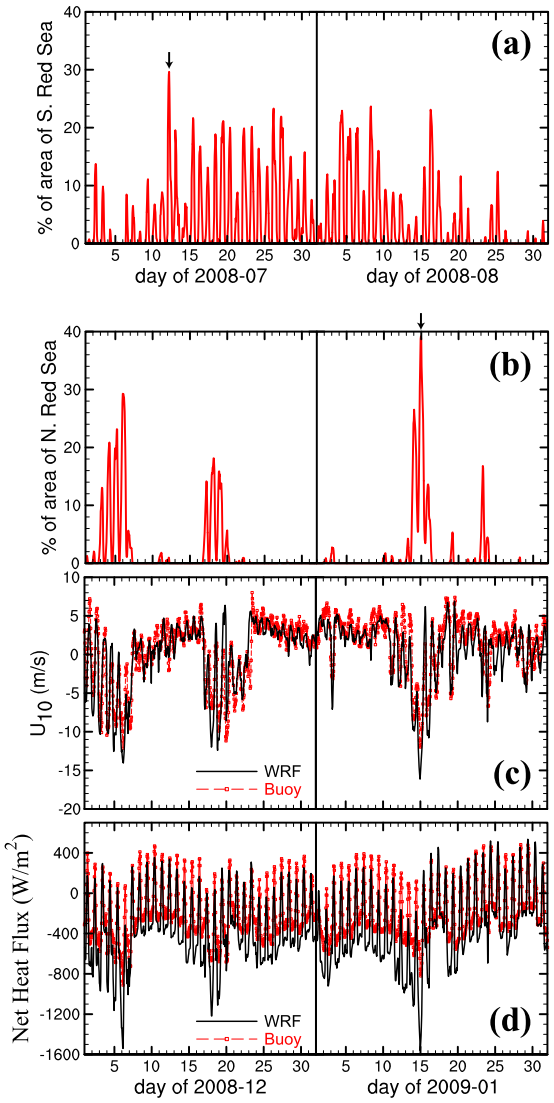

Figure 2. (a) Time series (July–August 2008) of the area percentage of the southern Red Sea (south of 20°N), over which the eastward 10-m zonal winds were greater than 10 m s^{-1}. The small black arrow indicates the time of 0500 UTC 12 July 2008. (b) Time series (December 2008 to January 2009) of the area percentage of the northern Red Sea (north of 20°N), over which the westward 10-m zonal winds were greater than 10 m s^{-1}. The small black arrow indicates the time of 2300 UTC 14 January 2009. Time series (December 2008 to January 2009) of buoy measured and WRF simulated (at the buoy location) (c) 10-m zonal winds and (d) net heat flux with negative values indicating ocean heat loss.

Atmospheric Prediction System (NORAPS), but the authors found that observed hydrographic variability (i.e., the eddy field) was better reproduced when the NORAPS winds were used to drive a higher-resolution atmospheric boundary layer model, which allowed for more realistic small-scale variability in the wind field caused by orographic effects. They further showed that the Red Sea water circulation was much more eddy-like when forced by strong cross-axis winds. Thus, there is a clear need for further investigation of the intensity, spatiotemporal variability, and occurrence frequency of the cross-axis zonal winds over the Red Sea.

[8] In the present study, the Weather Research and Forecasting (WRF) model with Advanced Research WRF (ARW) dynamic core version 3.0.1.1 [*Skamarock et al.*, 2008] is used to dynamically downscale the 1° NCEP Global Final Analysis (FNL) to a Red Sea subdomain. An approach of consecutive integrations with frequent (daily in this study) re-initializations [*Lo et al.*, 2008] is employed to run WRF from 1 December 2007 to 31 January 2009, generating an output dataset with hourly temporal and 10-km horizontal resolution. A few important results focusing on the cross-axis zonal winds are given here using the wind field of July–August 2008 and December 2008 to January 2009. These are the times when mountain gap winds are strongest, and they also correspond to the peaks of the two opposing monsoon seasons.

2. Results

[9] Both the July 2008 (Figure 1a) and January 2009 (Figure 1c) monthly vector mean 10-m surface wind fields show that the winds are not simply down the main axis but have significant cross-axis components and are rich in spatial variability. Particularly, the Tokar Gap funnels strong winds onto (out of) the Red Sea surface in summer (winter). Also computed are the monthly mean 10-m wind directional constancy fields, defined as the ratio of the magnitude of the monthly mean wind vector to the monthly mean wind speed [*Moore*, 2003]. Values near zero indicate unsteadiness in wind direction, whereas values near one indicate constancy in wind direction. In July, the wind jet near the Tokar Gap maintains high directional constancy along its jet-like spreading path, displaying a persistent cross-axis tendency (Figure 1b). In January, along the northeastern Red Sea coast, zones of (slightly) higher directional constancy are interspersed with those of lower directional constancy (Figure 1d). These higher constancy zones are collocated with the series of coastal mountain gaps (marked by blue arrows), indicating strong seaward wind jets channeled by these mountain gaps. These wind jets manifest themselves in the monthly mean wind field as the westward wind components along the Saudi Arabian coast north of 22°N (Figure 1c).

[10] From mid-June to mid-September, the Tokar Gap wind jet develops almost every day with a strong daily cycle of wind speed (Figure 2a). When the Tokar Gap wind jet is strongest, large areas of the Red Sea experience strong eastward winds. Up to 30% of the sea area south of 20°N can be covered by eastward 10-m zonal winds stronger than 10 m s^{-1} (Figure 2a) and maximum wind speed frequently reaches more than 15 m s^{-1} (Figure 3a).

[11] During the mountain gap wind events on the northeastern coast, almost 40% of the sea area north of 20°N can experience westward 10-m zonal winds stronger than 10 m s^{-1} (Figure 2b), attaining wind speeds greater than 15 m s^{-1} at times; the alternating surface jet and quieter zone (or even wake) pattern is evident (Figure 3b). These bands of westward-blowing mountain gap wind jets occur in wintertime (November–March) with an occurrence frequency of every 10–20 days (Figure 2b). When they happen, the wind jets can persist for several days, though

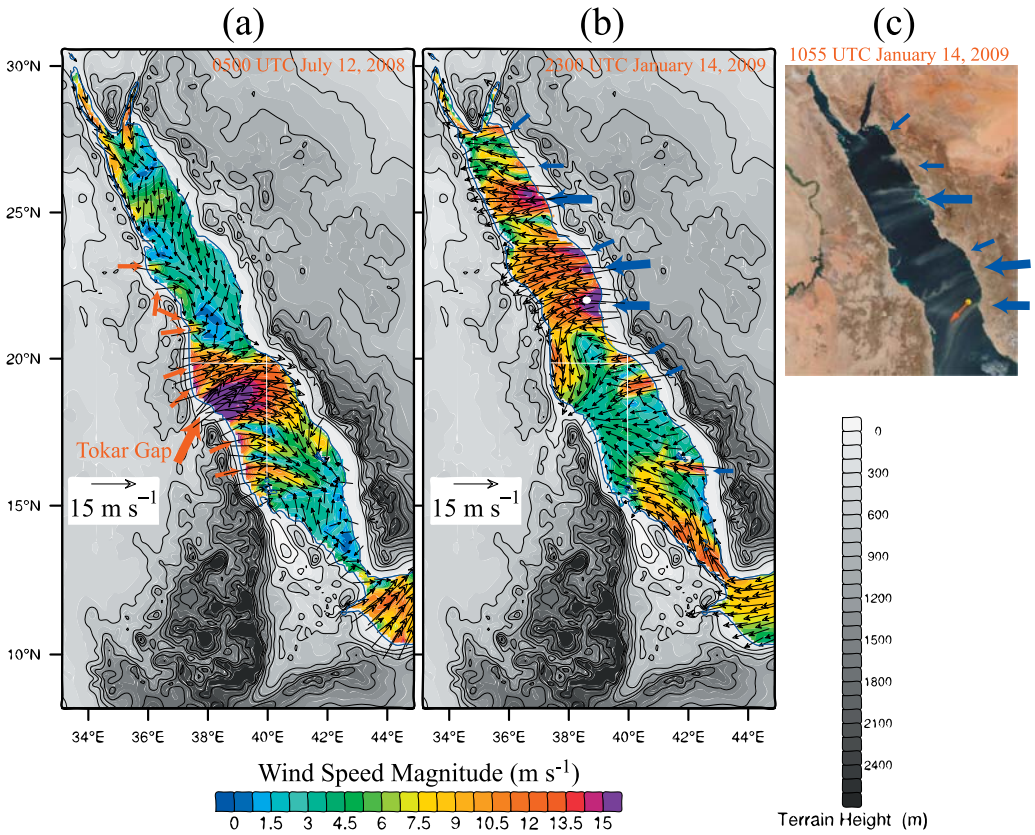

Figure 3. WRF model output of 10-m surface wind vector field overlapped with its magnitude (color contours) over the Red Sea region at (a) 0500 UTC 12 July 2008 and (b) 2300 UTC 14 January 2009. The wind vectors are shown for ~44 % of the grid points. (c) Dust plumes blew off the coast of Saudi Arabia and over the Red Sea in mid-January 2009. The Moderate Resolution Imaging Spectroradiometer (MODIS) on NASA's Aqua satellite captured this image at 1055 UTC 14 January 2009. The red arrows in Figure 3a indicate the locations of mountain gaps along the western coast of the Red Sea. The blue arrows in Figures 3b and 3c indicate the locations of mountain gaps along the eastern coast of the Red Sea. The white dot in Figure 3b and yellow dot in Figure 3c indicate the buoy location, and the red arrow in Figure 3c indicates the buoy wind direction.

with diurnal variability. Occurrence and timing of the wind jets are also confirmed by satellite imagery that shows dust plumes blowing off the coast with spatial patterns similar to the wind jets (Figure 3c).

[12] A moored meteorological buoy was deployed in the Red Sea near 22°10′N, 38°30′E, and surface meteorological measurements have been available via satellite telemetry since 11 October 2008 [*Farrar et al.*, 2009]. The WRF model results compare well with the buoy wind measurements (Figure 2c), and the good comparison is also confirmed by scatter plots (not shown). The buoy is located within one of the mountain gap wind jets along the northeastern coast (Figure 3b). Excellent alignment exists between occurrences of the wind jet events and buoy-recorded westward zonal wind speed peaks (Figure 2b versus Figure 2c). The wind-jet enhanced ocean heat loss can reach over 900 W m^{-2} as recorded by the buoy; the WRF model reproduces the general trend of the buoy-recorded net heat flux but overestimates the ocean heat loss during the wind jet events (Figure 2d). Such overestimating may be due to the fact that the NCEP daily data of 0.083° global SST analysis (RTG_SST_HR), which is input to WRF as the lower boundary condition, can be 1–2°C higher than the buoy measured SST especially during the wind jet events (not shown), thus making latent heat flux loss and long-wave radiation loss higher.

3. Discussion

[13] The Tokar Gap wind jet is a rather striking phenomenon in that it occurs almost daily in summertime normally from mid-June to mid-September. As soon as the wind jet develops, a high-speed wind patch spreads eastward across the southern Red Sea from midnight through early afternoon. The wind jet attains its maximum strength, frequently reaching over 15 m s^{-1}, around 0400–0600 UTC (Figures 2a and 3a). (Local time is UTC+3 for Saudi Arabia and Sudan.) At that time, because of nighttime radiative cooling over the semi-desert land, strong land-sea temperature contrasts develop and the resulting pressure drop seaward across the gap (see auxiliary material Figure S1a) drives strong nocturnal drainage airflow (also called katabatic wind [*Pielke*, 2002]).[1] Similar to the land/sea breeze mechanism, strong diurnal variability in the land-sea temperature contrasts leads to a clear daily cycle in the wind speed. However,

[1]Auxiliary materials are available in the HTML. doi:10.1029/2009GL040008.

the wind directional constancy remains high and there is virtually no landward blowing wind through the Tokar Gap. This is because from mid-June to mid-September the ground line position of the Inter-Tropical Convergence Zone (ITCZ) in Africa [*Pedgley*, 1974] migrates north of the Tokar Gap (see Figure S2) and subsequently a northeastward blowing wind persists in the region south to the gap. The vector sum of this northeastward blowing wind and the (landward) sea breeze is always seaward at the gap location. Therefore, the Tokar Gap wind jet forms when both the nocturnal drainage airflow and the summertime northeastward blowing wind are channeled through the Tokar Gap. A few weaker wind jets associated with a few smaller mountain gaps on the African coast can develop along side with the Tokar Gap wind jet (Figure 3a).

[14] Also revealed by the present WRF modeling study and confirmed by the buoy and satellite imagery are the bands of cross-Red Sea mountain gap wind jets along the northeastern coast. Their occurrences, every 10–20 days in wintertime, are causally related to synoptic-scale cold/dry-air outbreaks through those mountain gaps; when flowing downhill from the central plateau to the Red Sea coastal plain, the cold air experiences adiabatic compression (heating) and becomes 10–15°C warmer (see Figure S1b). The outbreaks may be due to local intensification of the Saudi Arabian High by radiative cooling in the desert of the northern Arabian Peninsula or by intrusion of cold, continental air flowing out of the wintertime Siberian High through the western passes of the Hindu Kush Mountains [*Naval Oceanography Command Detachment*, 1992]. These wind jets, especially their alternating jet and wake pattern, bear some similarities with the (wintertime occurring) northern Adriatic bora [*Pullen et al.*, 2003; *Dorman et al.*, 2006a]. In contrast to the above-described Red Sea wind jets, mountain gap channeled surface wind jets over the other marginal seas as the Adriatic or Japan/East [*Dorman et al.*, 2006b] Sea occur only during one part of the year and from one side/direction.

[15] Despite their differences in formation mechanism and occurrence timing, both types of coastal mountain gap wind jets contribute significantly to the monthly mean surface wind field and may be an important factor in the three-dimensional, time-dependent, eddy-rich circulation in the Red Sea. For example, the vigorous summer circulation pattern, specifically a series of strong anticyclones observed in the central sector of the Red Sea basin [*Sofianos and Johns*, 2007, Figure 9], could be correlated with the summertime occurrence of the Tokar Gap wind jet. The strong winds and dry desert air brought by the wintertime wind jet bands along the northeastern coast lead to enhanced evaporation and ocean heat loss, and their potential in driving deep convection warrants further investigation. Considering contributions by these wind jets to the wind and thermohaline forcing over the Red Sea is also important for our understanding of exchange between the Red Sea and the Indian Ocean [*Sofianos and Johns*, 2002, 2003] and for better wind resource assessment [*Van Buskirk et al.*, 1998].

[16] Both types of coastal mountain gap wind jets can drive dust storms/plumes over the Red Sea surface. Also revealed by this study is another strong zonal winds that blow from the Egyptian coast eastward across the Red Sea longitudinal axis (not shown). This type of zonal winds, although occurring less frequently, can also drive dust storms (satellite imagery not shown). The Tokar delta region on the Red Sea coast of Sudan is one of the two major Northern Hemisphere source regions for dust storm generation [*Hickey and Goudie*, 2007]. Thus, the Tokar Gap wind jets, which drive the Tokar delta dust storms, may have some global influences. Except for a few recent results on atmospheric dry deposits of nutrients over the Gulf of Aqaba [e.g., *Chen et al.*, 2007] and the inferred effects of high aerosol load over the Red Sea on surface heat flux budget [*Tragou et al.*, 1999], in general we lack a quantitative understanding of the role/importance of the Red Sea dust storms/plumes on nutrient supply, surface heat flux budget and sediment flux to the Red Sea.

[17] **Acknowledgments.** This study is part of a large research project on the Red Sea initialed in 2008 by King Abdullah University of Science and Technology (KAUST) and the Woods Hole Oceanographic Institution (WHOI). This short paper represents an initial contribution focusing on the Red Sea winds and is based on work supported by Award Numbers USA 00001, USA 00002, and KSA 00011 made by KAUST. We thank C. E. Dorman, S. J. Lentz, D. J. McGillicuddy, L. J. Pratt, and two anonymous reviewers for insightful comments. We thank J. Kemp, P. Bouchard, J. Smith, and B. Hogue of WHOI, the officers and crew of the R/V *Oceanus*, and Abdulaziz Al-Suwailem, Yasser Kattan, and Haitham Jahdali of KAUST for making the mooring work a success. HJ also acknowledges support from an Independent and Interdisciplinary Study Award provided by WHOI.

References

Chen, Y., S. Mills, J. Street, D. Golan, A. Post, M. Jacobson, and A. Paytan (2007), Estimates of atmospheric dry deposition and associated input of nutrients to Gulf of Aqaba seawater, *J. Geophys. Res.*, *112*, D04309, doi:10.1029/2006JD007858.

Clifford, M., C. Horton, J. Schmitz, and L. H. Kantha (1997), An oceanographic nowcast/forecast system for the Red Sea, *J. Geophys. Res.*, *102*, 25,101–25,122, doi:10.1029/97JC01919.

da Silva, A. M., C. C. Young, and S. Levitus (1994), *Atlas of surface marine data 1994, Vol. 1: Algorithms and Procedures, NOAA Atlas NESDIS 6*, 83 pp., Natl. Oceanic and Atmos. Admin., Washington, D. C.

Dorman, C. E., et al. (2006a), February 2003 marine atmospheric conditions and the bora over the northern Adriatic, *J. Geophys. Res.*, *111*, C03S03, doi:10.1029/2005JC003134 [printed *112*(C3), 2007].

Dorman, C. E., C. A. Friehe, D. Khelif, A. Scotti, J. Edson, R. C. Beardsley, R. Limeburner, and S. S. Chen (2006b), Winter atmospheric conditions over the Japan/East Sea: The structure and impact of severe cold-air outbreaks, *Oceanography*, *19*, 96–109.

Farrar, J. T., S. Lentz, J. Churchill, P. Bouchard, J. Smith, J. Kemp, J. Lord, G. Allsup, and D. Hosom (2009), King Abdullah University of Science and Technology (KAUST) mooring deployment cruise and fieldwork report, technical report, 88 pp., Woods Hole Oceanogr. Inst., Woods Hole, Mass.

Hickey, B., and A. S. Goudie (2007), The use of TOMS and MODIS to identify dust storm source areas: The Tokar delta (Sudan) and the Seistan basin (south west Asia), in *Geomorphological Variations*, edited by A. S. Goudie and J. Kalvoda, pp. 37–57, P3K, Prague.

Lo, J. C.-F., Z.-L. Yang, and R. A. Pielke Sr. (2008), Assessment of three dynamical climate downscaling methods using the Weather Research and Forecasting (WRF) model, *J. Geophys. Res.*, *113*, D09112, doi:10.1029/2007JD009216.

Moore, G. W. K. (2003), Gale force winds over the Irminger Sea to the east of Cape Farewell, Greenland, *Geophys. Res. Lett.*, *30*(17), 1894, doi:10.1029/2003GL018012.

Naval Oceanography Command Detachment (1992), U.S. Navy regional climatic study of the Persian Gulf and the northern Arabian Sea, *NAVAIR 50-1C-561*, Natl. Oceanic and Atmos. Admin., Asheville, N. C.

Naval Oceanography Command Detachment (1993), U.S. Navy regional climatic study of the Red Sea and adjacent waters, *NAVAIR 50-1C-562*, Natl. Oceanic and Atmos. Admin., Asheville, N. C.

Patzert, W. C. (1974), Wind-induced reversal in Red Sea circulation, *Deep Sea Res.*, *21*, 109–121.

Pedgley, D. E. (1974), An outline of the weather and climate of the Red Sea, in *L'Oceanographie Physique de la Mer Rouge*, pp. 9–27, U. N. Ed. Sci. and Cult. Org., Paris.

Pielke, R. A., Sr. (2002), *Mesoscale Meteorological Modeling*, 2nd ed., 676 pp., Academic, San Diego, Calif.

Pullen, J., J. D. Doyle, R. Hodur, A. Ogston, J. W. Book, H. Perkins, and R. Signell (2003), Coupled ocean-atmosphere nested modeling of the Adriatic Sea during winter and spring 2001, *J. Geophys. Res.*, *108*(C10), 3320, doi:10.1029/2003JC001780.

Quadfasel, D., and H. Baudner (1993), Gyre-scale circulation cells in the Red Sea, *Oceanol. Acta*, *16*, 221–229.

Skamarock, W. C., J. B. Klemp, J. Dudhia, D. O. Gill, D. M. Barker, M. G. Duda, X.-Y. Huang, W. Wang, and J. G. Powers (2008), A description of the advanced research WRF version 3, 113 pp., *NCAR Tech. Note NCAR/TN–475+STR*, Natl. Cent. for Atmos. Res., Boulder, Colo.

Sofianos, S. S., and W. E. Johns (2002), An Oceanic General Circulation Model (OGCM) investigation of the Red Sea circulation: 1. Exchange between the Red Sea and the Indian Ocean, *J. Geophys. Res.*, *107*(C11), 3196, doi:10.1029/2001JC001184.

Sofianos, S. S., and W. E. Johns (2003), An Oceanic General Circulation Model (OGCM) investigation of the Red Sea circulation: 2. Three-dimensional circulation in the Red Sea, *J. Geophys. Res.*, *108*(C3), 3066, doi:10.1029/2001JC001185.

Sofianos, S. S., and W. E. Johns (2007), Observations of the summer Red Sea circulation, *J. Geophys. Res.*, *112*, C06025, doi:10.1029/2006JC003886.

Tragou, E., C. Garrett, R. Outerbridge, and G. Gilman (1999), The heat and freshwater budgets of the Red Sea, *J. Phys. Oceanogr.*, *29*, 2504–2522, doi:10.1175/1520-0485[1999]029<2504:THAFBO>2.0.CO;2.

Van Buskirk, R., K. Garbesi, and K. Rosen (1998), Wind resource assessment of Eritrea, Africa: Preliminary results and status, *J. Wind Eng. Ind. Aerodyn.*, *74–76*, 365–374, doi:10.1016/S0167-6105(98)00033-6.

R. C. Beardsley, R. Chen, and J. T. Farrar, Department of Physical Oceanography, Woods Hole Oceanographic Institution, Woods Hole, MA 02543, USA.

C. Chen, School for Marine Science and Technology, University of Massachusetts-Dartmouth, New Bedford, MA 02744, USA.

H. Jiang, Department of Applied Ocean Physics and Engineering, Woods Hole Oceanographic Institution, Woods Hole, MA 02543, USA. (hsjiang@whoi.edu)

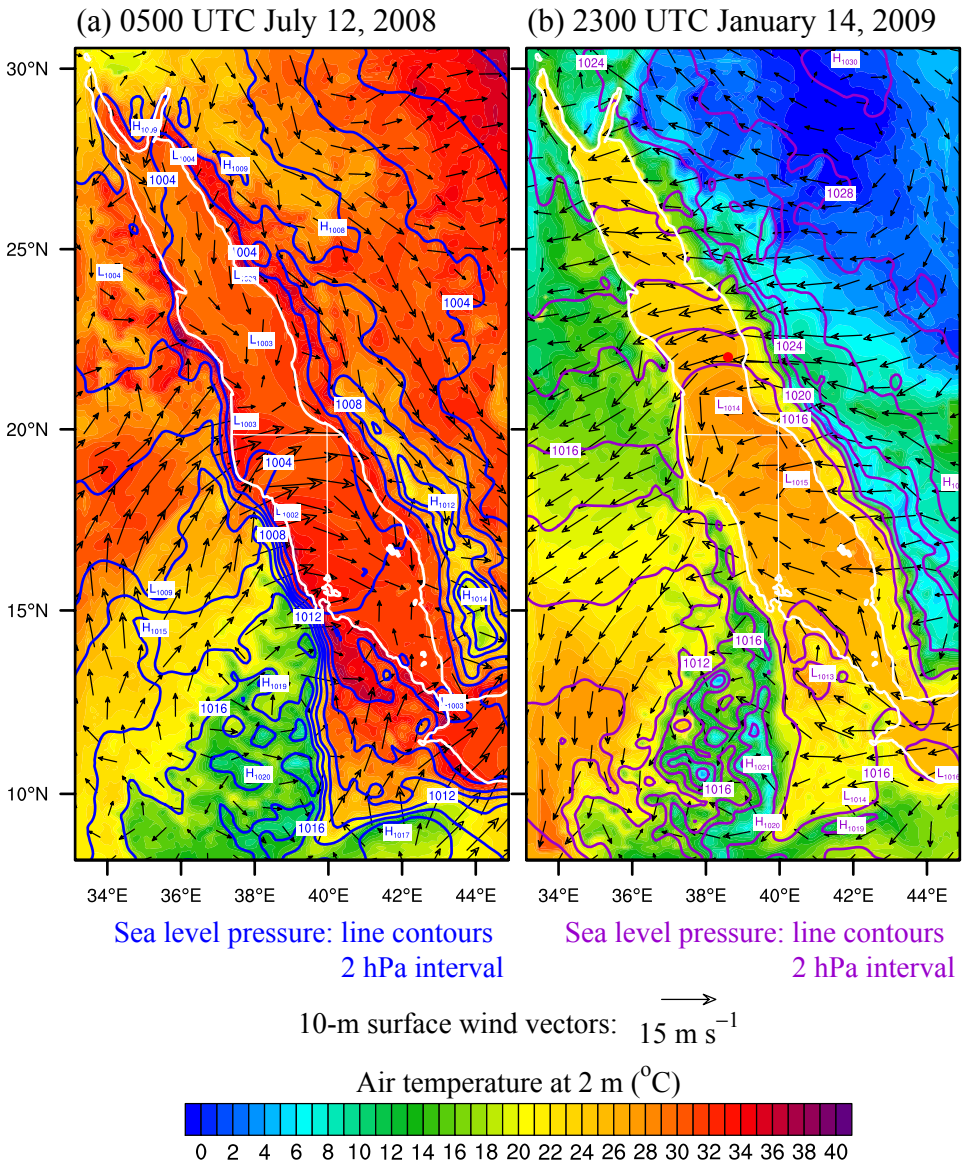

Figure S1 (auxiliary material). WRF model output of sea level pressure (line contours), 10-m surface wind vector field, and 2-m air temperature (color contours) over the Red Sea region, which give a sense of the larger-scale conditions leading to the two types of mountain gap wind jets. **(a)** 0500 UTC July 12, 2008. **(b)** 2300 UTC January 14, 2009. The red dot in (b) indicates the buoy location. The wind vectors are shown for ~20 % of the grid points.

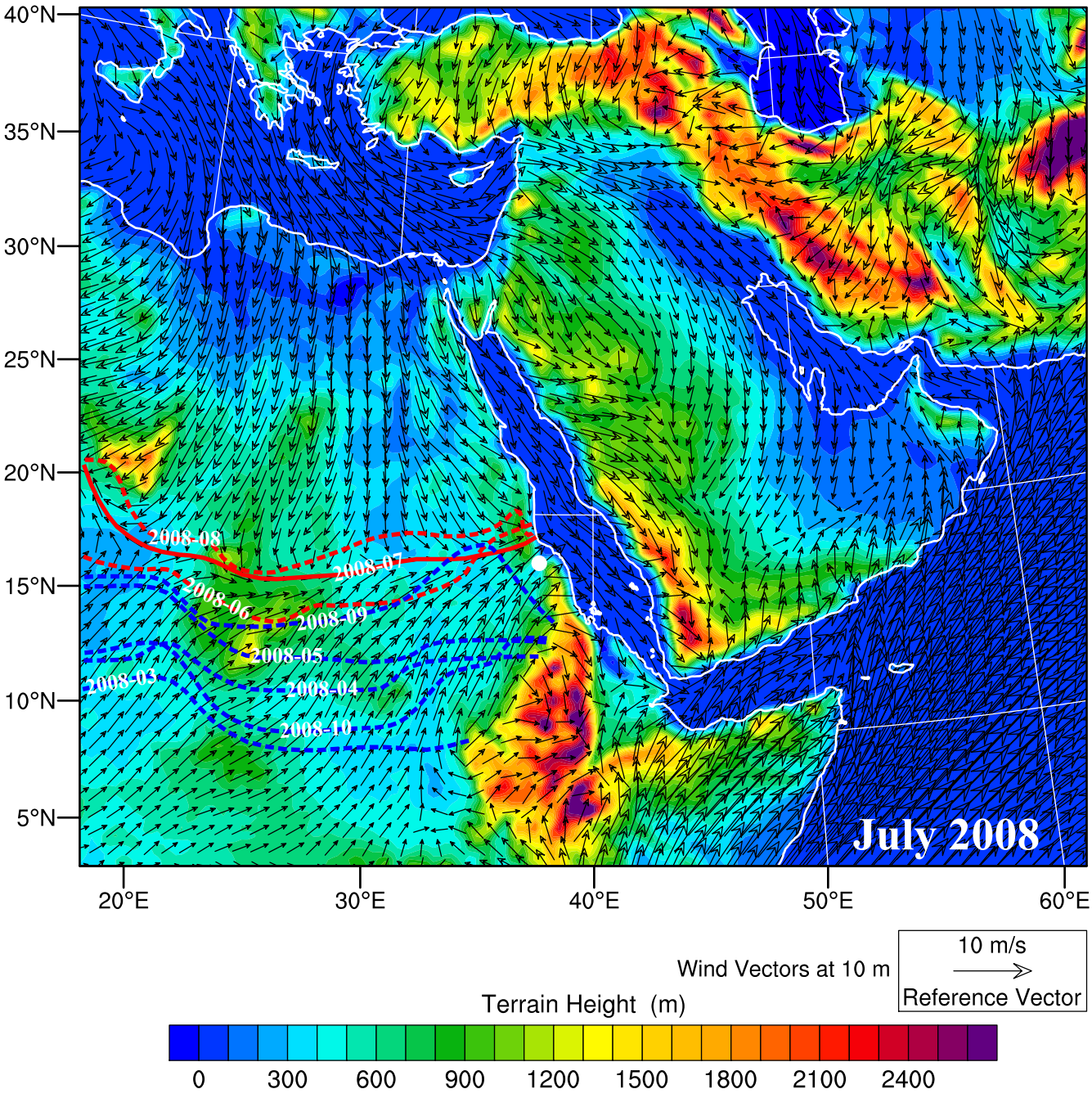

Figure S2 (auxiliary material). The red and blue lines show the monthly mean ground line positions of the Inter-Tropical Convergence Zone (ITCZ) in Africa, constructed from WRF model outputs (30-km horizontal resolution) of monthly mean 10-m surface winds over the Middle East for the months from March 2008 to October 2008. Also plotted is the July 2008 monthly mean 10-m surface wind vector field, overlapped with color contours of the terrain height. The big white dot indicates the location of the Tokar Gap (18.5^{o}N, 37.7^{o}E).